

Unveiling the microscopic nature of correlated organic conductors: the case of



Johannes Ferber, Kateryna Foyevtsova, Harald O. Jeschke,* and Roser Valenti†

*Institut für Theoretische Physik, Goethe-Universität Frankfurt,
Max-von-Laue-Strasse 1, 60438 Frankfurt/Main, Germany*

(Dated: September 13, 2021)

A few organic conductors show a diversity of exciting properties like Mott insulating behaviour, spin liquid, antiferromagnetism, bad metal or unconventional superconductivity controlled by small changes in temperature, pressure or chemical substitution. While such a behaviour can be technologically relevant for functional switches, a full understanding of its microscopic origin is still lacking and poses a challenge in condensed matter physics since these phases may be a manifestation of electronic correlation. Here we determine from first principles the microscopic nature of the electronic phases in the family of organic systems $\kappa\text{-(ET)}_2\text{Cu}[\text{N}(\text{CN})_2]\text{Br}_x\text{Cl}_{1-x}$ by a combination of density functional theory calculations and the dynamical mean field theory approach in a new form adapted for organic systems. By computing spectral and optical properties we are able to disentangle the origin of the various optical transitions in these materials and prove that correlations are responsible for relevant features. Remarkably, while some transitions are inherently affected by correlations, others are completely uncorrelated. We discuss the consequences of our findings for the phase diagram in these materials.

PACS numbers: 71.27.+a, 74.20.Pq, 74.70.Kn, 71.15.Ap, 74.25.Gz, 71.20.-b

One of the most intensively debated open questions in condensed matter physics is the emergence of exotic phases like spin liquid or unconventional superconductivity in a Mott insulator upon changes in temperature, doping or pressure. In particular, an increasingly prominent class of materials with an abundance of correlated phases are the κ -based organic charge transfer salts containing the molecules bis-(ethylenedithio)tetrathiafulvalene (BEDT-TTF, or shorter ET). In these $\kappa\text{-(ET)}_2X$ salts, electron donors (ET) and electron acceptors (X) form alternating layers, with pairs of ET molecules forming dimers $(\text{ET})_2$ arranged in a triangular lattice (see Figure 1). For monovalent anions X one electron is transferred from each dimer $(\text{ET})_2$ to each anion formula unit so that the system is half-filled. Band structure calculations [3, 4] therefore predict the dimer layers to be metallic. However, the experimentally observed ground state depends on the choice of the anion: even for the example of the isostructural compounds $\kappa\text{-(ET)}_2\text{Cu}[\text{N}(\text{CN})_2]\text{Cl}$ (in short $\kappa\text{-Cl}$) and $\kappa\text{-(ET)}_2\text{Cu}[\text{N}(\text{CN})_2]\text{Br}$ ($\kappa\text{-Br}$), the ground state can be as different as a Mott insulator for $\kappa\text{-Cl}$ and a Fermi liquid for $\kappa\text{-Br}$ at low temperatures and ambient pressure. [5] $\kappa\text{-Cl}$ can be driven through the insulator-to-metal transition (MIT) by the gradual substitution of Cl for isovalent Br. In the high-temperature regime $\kappa\text{-Cl}$ is a semiconductor with a gap of $E_g = 800$ K [7] while $\kappa\text{-Br}$ shows 'bad metal' behaviour with strong scattering preventing coherent transport and suppressing the Drude peak.

The fact that small chemical modifications lead to

qualitative changes in behaviour together with the possible importance of electronic correlations in these materials make it clear that a realistic description requires both (i) details of the band structure as well as (ii) a proper treatment of electronic correlations. However, many-body studies of the $\kappa\text{-(ET)}_2X$ salts have so far been limited to minimal model calculations [6, 8, 9] of the Hubbard or extended Hubbard Hamiltonian on an anisotropic triangular lattice. [10] In this work, we go beyond model calculations and present a combination of ab-initio density functional theory calculations in the full potential linearised augmented plane wave (FLAPW) framework [11] combined with DMFT [12] (local density approximation plus dynamical mean field theory, LDA+DMFT). Also, in order to perform these calculations for organic systems, we propose a generalisation of previously introduced Wannier projectors. [12]

We show that this first principles approach provides insight into the contributions to the optical conductivity at an unprecedented level; (i) we find that interdimer and intradimer transitions are responsible for two principal features resolved in optical conductivity measurements at low temperatures, (ii) we unambiguously identify the interdimer feature to be related to correlations and (iii) we are able to unveil the origin of the anisotropic conductivity (light polarisation-dependent). These calculations go beyond previous conjectures based on phenomenological and minimal model assumptions. [13, 14]

While recent LDA+DMFT calculations on organic molecular crystals employed Wannier functions with a single atomic character, [15] the electronic structure of organic charge transfer salts requires the construction of localised Wannier functions from the entire highest occupied molecular orbital (HOMO). A fast and stable method to obtain Wannier functions consists in project-

*Electronic address: jeschke@itp.uni-frankfurt.de

†Electronic address: valenti@itp.uni-frankfurt.de

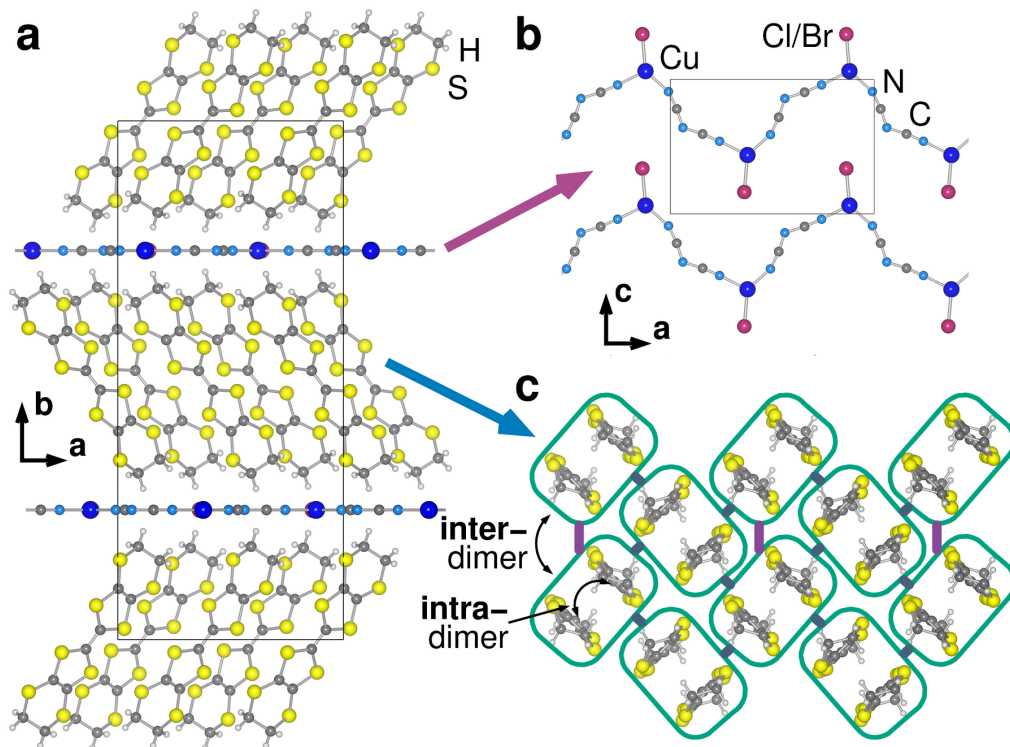


FIG. 1: **a** Structure of κ -(ET) $_2$ Cu[N(CN) $_2$]Cl/Br seen in the ab plane. **b**, **c** Separate anion and cation layers projected in the ac plane.

ing Bloch states onto pure atomic orbitals with subsequent orthonormalization. [12, 16, 17] In its standard form, though, this method is not designed for molecular orbitals. In this work, we propose a scheme to construct molecular Wannier functions using atomic orbitals as a starting point. The key element of this scheme is the diagonalization of the occupation matrix written in the basis of atomic orbitals within the subspace of the correlated bands. [18] The real space representation of the resulting dimer HOMO Wannier function of κ -Cl (based on the crystal structure reported in Ref. 19 with space group $Pnma$) is shown in Fig. 2. Once the Wannier functions are obtained out of the LDA cycle, we employ the hybridisation expansion continuous-time quantum Monte Carlo method [20] as implemented in the ALPS code [21, 22] in order to solve the impurity problem in the DMFT cycle. We used 2×10^7 Monte Carlo sweeps throughout our calculations at an inverse temperature $\beta = 40 \text{ eV}^{-1}$, corresponding to room temperature $T = 300 \text{ K}$. Since the quantum Monte Carlo algorithm operates on the imaginary frequency axis, the calculation of dynamical quantities like spectral functions and optical conductivity requires analytic continuation to the real axis. We performed stochastic analytic continuation [24] on the self energy for obtaining the spectral functions and directly on the optical conductivity $\sigma(i\nu)$ for the calculation of optical properties. [18]

In Fig. 3 **a-b** we show the LDA+DMFT calculated

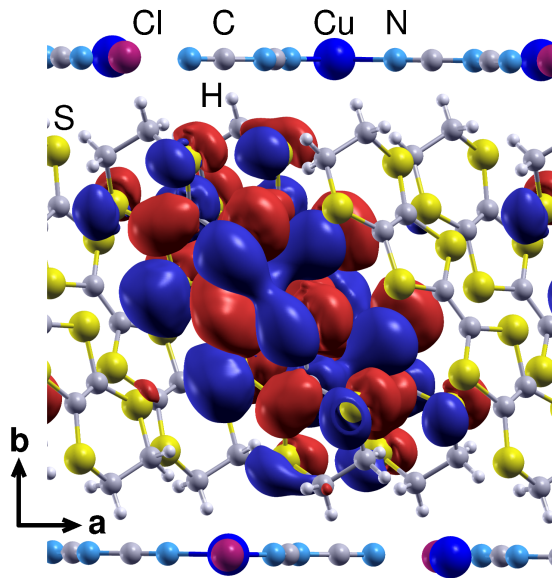


FIG. 2: Structure of κ -(ET) $_2$ Cu[N(CN) $_2$]Cl seen in the ab plane with a Wannier function corresponding to the bands crossing the Fermi level.

band structure [23] of κ -(ET) $_2$ Cu[N(CN) $_2$]Br $_x$ Cl $_{1-x}$ in form of the momentum-resolved spectral function for Hubbard $U = 0.6 \text{ eV}$ (Fig. 3 **b**) along with the LDA band energies (3 **a**). The LDA calculations were done

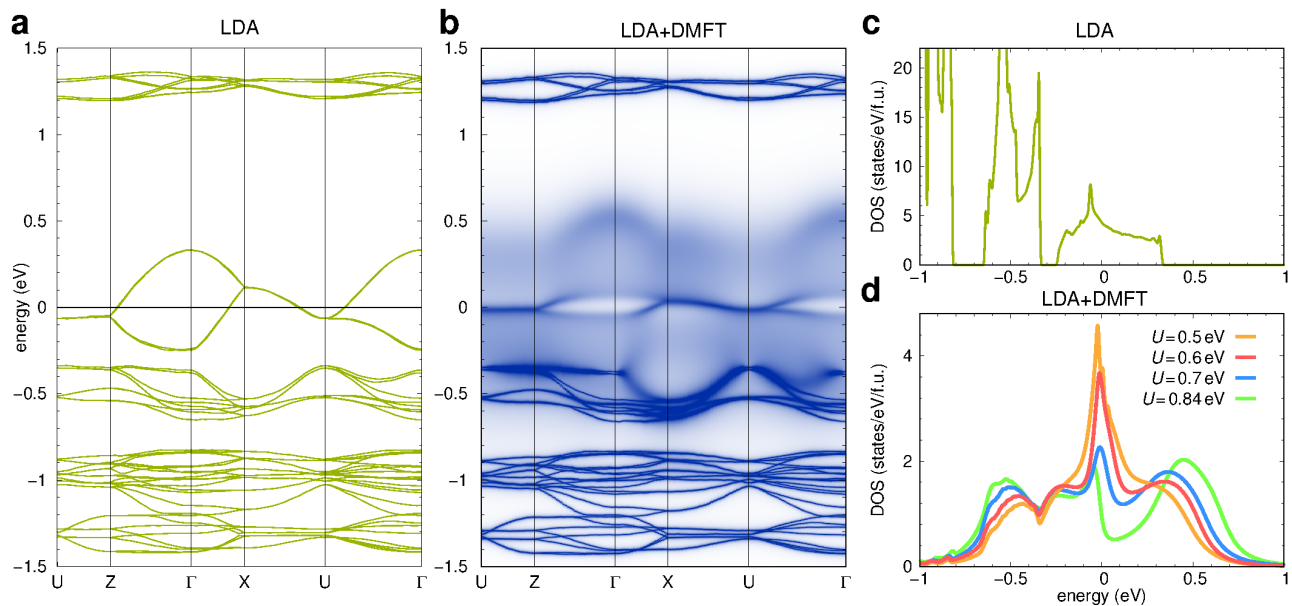


FIG. 3: **a** LDA Bandstructure of κ -(ET) $_2$ Cu[N(CN) $_2$]Cl. **b** LDA+DMFT momentum-resolved spectral function for $U = 0.6$ eV. Note that the LDA+DMFT results are not sharp since the spectral function $A(k, \omega)$ is not a delta function. **c** LDA density of states, and **d** LDA+DMFT DOS (\mathbf{k} integrated spectral function, for the projected manifold) for different values of the interaction strength U .

for the stoichiometric κ -Cl and κ -Br. We find only small changes of the LDA bandstructure [3] at E_F between both systems. The choice of $U = 0.6$ eV in the LDA+DMFT calculations is guided by two estimates: $U = 0.85$ eV obtained for a similar but arguably more strongly correlated compound κ -(ET) $_2$ Cu $_2$ (CN) $_3$ from constrained random phase approximation, [4] and $U \approx 0.27$ eV extracted from optical conductivity measurements [13] and model considerations. [9] The LDA+DMFT bands (Fig. 3 b) show a strong renormalisation at $E_F = 0$ with respect to the LDA bands (Fig. 3 a). These bands originate from the interdimer hopping (see Fig. 1 c), in particular hopping between dimers on the same layer; the interlayer hopping is very small, so that the four bands are composed of two almost degenerate pairs of bands. The correlation in band space acts almost exclusively on these bands, splitting them into renormalized excitations of (mass-enhanced) quasiparticles (blue-scale colour map at $E_F = 0$) and a spectral weight transfer to an upper and lower Hubbard band which manifests itself as blurry background around -0.5 eV and 0.5 eV respectively. On the other hand, the charge transfer between the ET molecules within a dimer (intradimer, see Fig. 3 c) induces the splitting between the bands into bonding (around -0.4 eV) and antibonding bands (around the Fermi level). This splitting is less affected by correlations as can be observed by comparing Fig. 3 a and b.

Next, we investigate the optical properties of κ -(ET) $_2$ Cu[N(CN) $_2$]Br $_x$ Cl $_{1-x}$ first with the light polarisation $\mathbf{E} \parallel \mathbf{c}$ along the linear chains in the triangular lattice as measured experimentally. [13, 14] At room temperature, the authors of Ref. 13 observed a broad mid-infrared

absorption peak between 1600 cm^{-1} and 4200 cm^{-1} , in agreement with previous optical studies on κ -Cl and κ -Br (see Ref. 13 and references therein). At low temperature, a Drude peak evolves for the compounds with high Br concentration which marks the onset of metallicity at $x \approx 0.7$ whereas no Drude peak is visible for lower Br content indicating an insulating state without coherent quasiparticles. Importantly, at low temperatures ($T=90$ K and below) the broad mid-infrared peak (polarisation $\mathbf{E} \parallel \mathbf{c}$) splits into two peaks in the pure Cl and low Br concentration compounds, which can be fitted by two Lorentzians at ≈ 2200 cm^{-1} and 3200 cm^{-1} ; for high Br content this splitting is very weak but it is still present. From this doping dependence, it was suggested [13] that the first peak is a correlation-induced feature due to electron transitions between the lower and upper Hubbard bands, while the second peak was assigned to the intradimer charge transfer (see Fig. 8 of Ref. 13). In contrast, for polarisation $\mathbf{E} \parallel \mathbf{a}$ the broad mid-infrared peak doesn't show any splitting at low temperatures. This anisotropic behaviour of the optical conductivity has remained unresolved up to now.

The method introduced in this work allows us to investigate the microscopic origin of the observed spectra. As the energy window of our LDA+DMFT calculation contains both the correlated manifold at the Fermi energy as well as uncorrelated bands away from E_F , all transitions can be inspected on equal footing. Our calculations are at $T=300$ K (continuous-time QMC) and capture the effects of correlation contained in the $T=300$ K data and observed as pronounced features in measurements below room temperature. We denote the transitions occurring

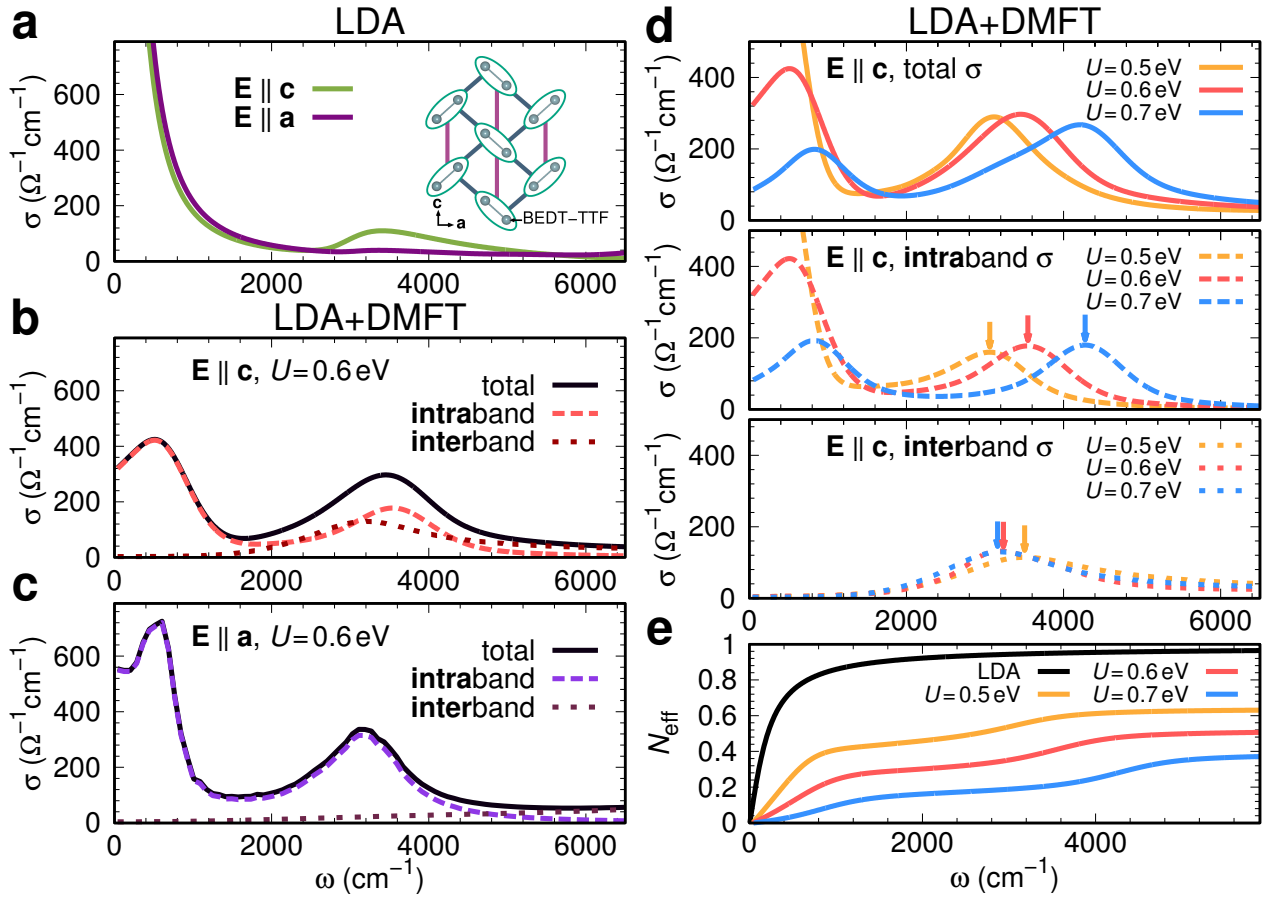


FIG. 4: **a** Calculated LDA optical conductivity for two directions of the light polarisation. **b** and **c** LDA+DMFT optical conductivity for $U = 0.6$ eV for electrical field along **a** and **c**, respectively. **d** LDA+DMFT optical conductivity for different values of the interaction strength U . The arrows show the position of maxima for the intraband (middle panel) and the interband (lower panel) contributions. **e** Optical conductivity sum rule for LDA and LDA+DMFT at different U values.

at the Fermi level between (i) Hubbard bands and (ii) Hubbard bands and quasiparticle peak (if present) as *intra*band contributions (i.e. *inter*dimer transitions) to the optical conductivity. All other transitions are termed *inter*band transitions; among others, these contain transitions related to the *intra*dimer charge transfer.

In Fig. 4 **a-c** we show the LDA and LDA+DMFT ($U = 0.6$ eV) calculated optical conductivity for polarisation $\mathbf{E} \parallel \mathbf{c}$ and $\mathbf{E} \parallel \mathbf{a}$. We would like to note that while the LDA results change minimally between κ -Cl and κ -Br, they are extremely sensitive to the effects of correlation (U) as can be observed in the density of states (Fig. 3 **c-d**) and in the optical conductivity (Fig. 4 **d**). For $U > 0.84$ eV a gap opens and the Drude peak disappears. This corresponds to the κ -Cl system although with a somewhat overestimated U value (this is a well-known limitation of single-site DMFT in low dimensions [9]). Smaller U values feature the conductivity behaviour of κ -(ET)₂Cu[N(CN)₂Br_xCl_{1-x}] at larger values of x . For $U = 0.6$ eV we observe a remnant of the Drude peak as it is the case in κ -(ET)₂Cu[N(CN)₂Br_xCl_{1-x}] at moderate x .

For $\mathbf{E} \parallel \mathbf{c}$ the calculated LDA+DMFT total optical conductivity (Fig. 4 **b**) features one dominant low-frequency peak at approximately 3450 cm^{-1} , i.e., close to the experimental peak position (we do not consider vibronic modes). [13] The position of this peak is roughly centred at the same position as the LDA results (Fig. 4 **a**), but it is strongly enhanced in spectral weight, in accordance with experiment. [13] While our calculations are at room temperature, they already capture the effects of correlation resolved in measurements at low T. We can decompose our data into intra- and interband contributions. $\sigma_{\text{interband}}$ contains contributions of transitions between almost uncorrelated bands and roughly coincides with the LDA results in position and spectral weight. This contribution shows a peak at $\omega \approx 3400 \text{ cm}^{-1}$ that corresponds to *intra*dimer transitions (Fig. 4 **b** dotted line). In contrast, the intraband contribution σ_{intra} is centred at $\omega \approx 3550 \text{ cm}^{-1} \approx 0.75 U$ and it corresponds to the intraband Hubbard transitions (*inter*dimer contribution, Fig. 4 **b** dashed line). Once thermal fluctuations are suppressed by lowering temperature, the two low frequency contributions (3400 cm^{-1} and 3550 cm^{-1}) –that

come naturally out of our calculations– are experimentally observed as two distinguishable peaks, a ”dimer” peak and a ”Hubbard” peak respectively. [13]

In order to analyse the nature of the two low-frequency intraband and interband absorption peaks, Fig. 4 d shows their evolution with U . The intraband contribution (interdimer transitions) to the conductivity shifts in frequency proportional to U , with the peak position consistently corresponding to $\approx 0.75U$ while the interband absorption peak at low frequencies (intradimer transitions) is largely insensitive to U . This analysis demonstrates the correlated nature of $\sigma_{\text{intraband}}$ and uncorrelated nature of $\sigma_{\text{interband}}$.

Quantitatively, the suppression of the Drude peak as a function of U and the redistribution of the intraband spectral weight is presented in Fig. 4 e where we plot the integrated spectral weight $\int_0^\omega \sigma_{\text{intraband}}(\omega')d\omega'$ representing the effective number of charge carriers N_{eff} . In this representation, the number of charge carriers in LDA by definition equals the number of conduction electrons, *i. e.* one, and all the weight is concentrated in the (infinitesimally narrow) coherent Drude peak which is only broadened by temperature. Upon inclusion of correlations, the kinetic energy of the electrons is diminished, which corresponds to a mass enhancement (in Fermi liquid theory) or a reduction of the number of effective charge carriers as we observe.

Summarising the above analysis, we have shown from first principles that the two finite-frequency peaks resolved in the experimental optical conductivity for $\mathbf{E} \parallel \mathbf{c}$ of $\kappa\text{-(ET)}_2\text{Cu}[\text{N}(\text{CN})_2]\text{Br}_x\text{Cl}_{1-x}$ at low temperatures originate, respectively, from correlation-induced intraband (interdimer) contributions scaling with U , and interband (intradimer) transitions which are unaffected by correlations. The fact that DMFT overestimates the critical U of the triangular lattice in two dimensions forces us to describe these systems at $T=300$ K with a somewhat high interaction strength of $U = 0.6$ eV.

We focus now on the optical conductivity $\mathbf{E} \parallel \mathbf{a}$. The LDA optical conductivity is completely featureless for $\omega \approx 3400 \text{ cm}^{-1}$ (Fig. 4 a). Inclusion of correlation effects (Fig. 4 c) shows the appearance of a peak at this frequencies. This peak is therefore only a consequence of transitions between the lower Hubbard band/quasiparticle peak and the upper Hubbard band (interdimer contribution) and at low temperatures no splitting of the peak is therefore to be expected, as observed experimentally [13], in contrast to the $\mathbf{E} \parallel \mathbf{c}$ case. Finally we would like to note that while calculations were performed at $T=300$ K, important information was obtained for the features observed at lower temperatures. Accurate calculations of the optical conductivity at lower temperatures requires the use of alternative impurity solvers [30] and is beyond the scope of the present study.

In conclusion, we presented the first LDA+DMFT study on the spectral and optical properties of the organic charge transfer salts $\kappa\text{-(ET)}_2\text{Cu}[\text{N}(\text{CN})_2]\text{Br}_x\text{Cl}_{1-x}$. Our results provide an *ab initio*-based theoretical evidence for the double-natured origin of the infrared peak in the optical conductivity of this system for $\mathbf{E} \parallel \mathbf{c}$ as well as for the single-natured origin of the infrared peak for $\mathbf{E} \parallel \mathbf{a}$. We could identify intraband transitions within the correlated manifold and interband transitions due to charge-transfer within an ET dimer. The proposed projection method for constructing non-atom-centred Wannier functions in the FLAPW framework is computationally efficient and can be applied to a great variety of correlated organic as well as inorganic systems with (quasi-)molecular orbitals. This opens the possibility of investigating correlation effects in complex organic systems from first principles.

Acknowledgements.- We acknowledge useful discussions with M. Dressel. We gratefully acknowledge financial support from the Deutsche Forschungsgemeinschaft through TR49 and FOR1346 and the allotment of computer time by CSC-Frankfurt and LOEWE-CSC.

-
- [1] K. Kanoda and R. Kato, *Mott Physics in Organic Conductors with Triangular Lattices*, Annu. Rev. Condens. Matter Phys. **2**, 167 (2011).
- [2] B. J. Powell and R. H. McKenzie, *Quantum frustration in organic Mott insulators: from spin liquids to unconventional superconductors*, Rep. Prog. Phys. **74**, 056501 (2011).
- [3] H. C. Kandpal, I. Opahle, Y.-Z. Zhang, H. O. Jeschke and R. Valentí, *Revision of Model Parameters for κ -Type Charge Transfer Salts: An Ab Initio Study*, Phys. Rev. Lett. **103**, 067004 (2009).
- [4] K. Nakamura, Y. Yoshimoto, T. Kosugi, R. Arita, and M. Imada, *Ab initio Derivation of Low-Energy Model for κ -ET Type Organic Conductors*, J. Phys. Soc. Jpn. **78**, 083710 (2009).
- [5] Below 35 K, $\kappa\text{-(ET)}_2\text{Cu}[\text{N}(\text{CN})_2]\text{Cl}$ develops a weak magnetic order [27, 28] whereas $\kappa\text{-(ET)}_2\text{Cu}[\text{N}(\text{CN})_2]\text{Br}$ enters a superconducting state at $T_c = 12$ K. [29] We are not considering these very low temperature phases here.
- [6] J. Merino, R. H. McKenzie, *Transport properties of strongly correlated metals: A dynamical mean-field approach*, Phys. Rev. B **61**, 7996 (2000).
- [7] S. Yasin, M. Dumm, B. Salameh, P. Batail, C. Mézière and M. Dressel, *Transport studies at the Mott transition of the two-dimensional organic metal $\kappa\text{-(ET)}_2\text{Cu}[\text{N}(\text{CN})_2]\text{Br}_x\text{Cl}_{1-x}$* , Eur. Phys. J. B **79**, 383 (2011).
- [8] O. Parcollet, G. Biroli and G. Kotliar, *Cluster Dynamical Mean Field Analysis of the Mott Transition*, Phys. Rev. Lett. **92**, 226402 (2004).
- [9] J. Merino, M. Dumm, N. Drichko, M. Dressel and R. H. McKenzie, *Quasiparticles at the Verge of Localization near the Mott Metal-Insulator Transition in a Two-Dimensional Material*, Phys. Rev. Lett. **100**, 086404 (2008).
- [10] B. J. Powell and R. H. McKenzie, *Strong electronic corre-*

- lations in superconducting organic charge transfer salts, *J. Phys.: Condens. Matter* **18**, R827 (2006).
- [11] P. Blaha, K. Schwarz, G. K. H. Madsen, D. Kvasnicka, & J. Luitz, WIEN2k, An Augmented Plane Wave + Local Orbitals Program for Calculating Crystal Properties (Techn. Universität Wien, Austria, 2001).
- [12] M. Aichhorn, L. Pourovskii, V. Vildosola, M. Ferrero, O. Parcollet, T. Miyake, A. Georges and S. Biermann, *Dynamical mean-field theory within an augmented plane-wave framework: Assessing electronic correlations in the iron pnictide LaFeAsO*, *Phys. Rev. B* **80**, 085101 (2009).
- [13] D. Faltermeier, J. Barz, M. Dumm, M. Dressel, N. Drichko, B. Petrov, V. Semkin, R. Vlasova, C. Mézière and P. Batail, *Bandwidth-controlled Mott transition in κ -(ET)₂Cu[N(CN)₂]Br_xCl_{1-x}: Optical studies of localized charge excitations*, *Phys. Rev. B* **76**, 165113 (2007).
- [14] M. Dumm, D. Faltermeier, N. Drichko, M. Dressel, C. Mézière and P. Batail, *Bandwidth-controlled Mott transition in κ -(ET)₂Cu[N(CN)₂]Br_xCl_{1-x}: Optical studies of correlated carriers*, *Phys. Rev. B* **79**, 195106 (2009).
- [15] C. Weber, D. D. O'Regan, N. D. M. Hine, P. B. Littlewood, G. Kotliar and M. C. Payne, *Importance of Many-Body Effects in the Kernel of Hemoglobin for Ligand Binding*, *Phys. Rev. Lett.* **110**, 106402 (2013).
- [16] W. Ku, H. Rosner, W. E. Pickett and R. T. Scalettar, *Insulating Ferromagnetism in La₄Ba₂Cu₂O₁₀: An Ab Initio Wannier Function Analysis*, *Phys. Rev. Lett.* **89**, 167204 (2002).
- [17] V. I. Anisimov, D. E. Kondakov, A. V. Kozhevnikov, I. A. Nekrasov, Z. V. Pchelkina, J. W. Allen, S.-K. Mo, H. D. Kim, P. Metcalf, S. Suga, A. Sekiyama, G. Keller, I. Leonov, X. Ren and D. Vollhardt, *Full orbital calculation scheme for materials with strongly correlated electrons*, *Phys. Rev. B* **71**, 125119 (2005).
- [18] See the Supplementary Material for a detailed description of the method.
- [19] J. M. Williams, A. M. Kini, H. H. Wang, K. D. Carlson, U. Geiser, L. K. Montgomery, G. J. Pyrka, D. M. Watkins, J. M. Kommers, S. J. Boryscuk, A. V. S. Crouch, W. K. Kowk, J. E. Schirber, D. L. Overmyer, D. Jung and M.-H. Whangbo, *From Semiconductor-Semiconductor Transition (42 K) to the Highest-T_c Organic Superconductor, κ -(ET)₂Cu[N(CN)₂]Cl (T_c = 12.5 K)*, *Inorg. Chem.* **29**, 3272-3274 (1990).
- [20] P. Werner, A. Comanac, L. de' Medici, M. Troyer and A. J. Millis, *Continuous-Time Solver for Quantum Impurity Models*, *Phys. Rev. Lett.* **97**, 076405 (2006).
- [21] B. Bauer, L. D. Carr, H. G. Evertz, A. Feiguin, J. Freire, S. Fuchs, L. Gamper, J. Gukelberger, E. Gull, S. Guertler, A. Hehn, R. Igarashi, S. V. Isakov, D. Koop, P. N. Ma, P. Mates, H. Matsuo, O. Parcollet, G. Pawłowski, J. D. Picon, L. Pollet, E. Santos, V. W. Scarola, U. Schollwöck, C. Silva, B. Surer, S. Todo, S. Trebst, M. Troyer, M. L. Wall, P. Werner and S. Wessel, *The ALPS project release 2.0: open source software for strongly correlated systems*, *J. Stat. Mech.*, P05001 (2011).
- [22] E. Gull, P. Werner, S. Fuchs, B. Surer, T. Pruschke and M. Troyer, *Continuous-time quantum Monte Carlo impurity solvers*, *Comp. Phys. Commun.* **182**, 1078 (2011).
- [23] Note that in the crystallographic unit cell, there is a manifold of four bands around E_F as the crystallographic unit cell contains two organic layers with a total of four dimers due to the presence of the anion. The dimers are equivalent, though, so that only one dimer HOMO has to be considered in our single-site DMFT; the other three orbitals are related by symmetry.
- [24] K. S. D. Beach, *Identifying the maximum entropy method as a special limit of stochastic analytic continuation*, arXiv:cond-mat/0403055 (unpublished).
- [25] P. Sahebsara and D. Sénéchal, *Hubbard Model on the Triangular Lattice: Spiral Order and Spin Liquid*, *Phys. Rev. Lett.* **100**, 136402 (2008).
- [26] H. Lee, K. Foyevtsova, J. Ferber, M. Aichhorn, H. O. Jeschke and R. Valentí, *Dynamical cluster approximation within an augmented plane wave framework: Spectral properties of SrVO₃*, *Phys. Rev. B* **85**, 165103 (2012).
- [27] K. Miyagawa, A. Kawamoto, Y. Nakazawa and K. Kanoda, *Antiferromagnetic Ordering and Spin Structure in the Organic Conductor κ -(ET)₂Cu[N(CN)₂]Cl*, *Phys. Rev. Lett.* **75**, 1174 (1995).
- [28] K. Kanoda, *Electron Correlation, Metal-Insulator Transition and Superconductivity in Quasi-2D Organic Systems, (ET)₂X*, *Physica C* **282-287**, 299 (1997).
- [29] A. M. Kini, U. Geiser, H. H. Wang, K. D. Carlson, J. M. Williams, W. K. Kwok, K. G. Vandervoort, J. E. Thompson and D. L. A. Stupka, *New Ambient-Pressure Organic Superconductor, κ -(ET)₂Cu[N(CN)₂]Br, with the Highest Transition Temperature Yet Observed (Inductive Onset T_c = 11.6 K, Resistive Onset = 12.5 K)*, *Inorg. Chem.* **29**, 2555 (1990).
- [30] Xiaoyu Deng, Jernej Mravlje, Rok Zitko, Michel Ferrero, Gabriel Kotliar, Antoine Georges, *Phys. Rev. Lett.* **110**, 086401 (2013).